Table 2 | Allelic frequencies of non-synonymous mutations in the *ZIC2* gene in patients with schizophrenia and control subjects.

| | Control | | | | Schizophrenia | | | | |
|---|---|---|---|---|---|---|---|---|---|
| Polymorphism | Genotype count | | | MAF[2] | Genotype count | | | MAF | Polyphen (PSIC)[1] |
| Ala95Thr (283G>A) | G/G | G/A | A/A | 0 | G/G | G/A | A/A | 0.041 | Benign (0.897) |
| | 1,036 | 0 | 0 | | 1,226 | 1 | 0 | | |
| Ins239His | del/del | del/ins | ins/ins | 8.95 | del/del | del/ins | ins/ins | 8.77 | |
| | 865 | 173 | 7 | | 1,025 | 198 | 9 | | |
| Arg409Pro | G/G | G/C | C/C | 0 | G/G | G/C | C/C | 0.04 | Probably damaging (2.745) |
| (1,226G>C) | 1,058 | 0 | 0 | | 1,238 | 1 | 0 | | |
| Ser444Arg | C/C | C/A | A/A | 0.284 | C/C | C/A | A/A | 0.363 | Possibly damaging (1.541) |
| (1,332C>A) | 1,051 | 6 | 0 | | 1,230 | 9 | 0 | | |

[1]Polyphen is a computer algorithm used to predict the effects of non-synonymous single-nucleotide polymorphisms (SNPs) on protein structure and function [30]. PSIC, difference in position-specific independent counts.
[2]MAF, minor allele frequency

sensorimoter-gating function seen in schizophrenia, is reported in $Zic2^{kd/+}$ [12]. These results corroborate that the cognitive function deficits in $Zic2^{kd/+}$ mice are not simple, but multimodal ones including sensorimotor gating function.

Social behavioral abnormalities in $Zic2^{kd/+}$ mice were characterized by a reduction in aggressive behavior compared to the wild-type controls in the absence of clear deficits in the affiliative behaviors. The aggressivity assessed in the resident-intruder and social dominance tube tests may be related to their territory protecting behavior. The absence of depression-like behavior in these mice excludes the possibility that their reduced aggressivity was the result of a general loss in motivation.

Collectively, the behavioral phenotypes of $Zic2^{kd/+}$ mice seem to be implicated in the three classes of schizophrenia symptoms (positive/negative symptoms and cognitive dysfunction). When we compare the $Zic2^{kd/+}$ mice phenotype with those of other typical schizophrenia model mice (Table 3), novelty-induced hyperactivity and prepulse inhibition reduction were commonly found in the dominant negative DISC1 transgenic[38]and NRG1 transmembrane KO[35]and conditional KO of ErbB4 in PV-positive interneuron[39]. In addition, the enlargement of lateral ventricle and decrement of working memory were shared with $Zic2^{kd/+}$ and some of them (Table 3).

The morphological abnormalities in the brain of $Zic2^{kd/}$ include a reduction in the septal mass, thinning of the cerebral cortex and corpus callosum, narrowing of the fimbria hippocampi, and a regional reduction of amygdalar nuclei. These abnormalities have a pathophysiological resemblance to neuropsychiatric disorders in humans. In particular, enlarged lateral ventricles and decrease in whole brain volume are a symptom of the first episode of schizophrenia[16–18], and have been observed in some genetically-engineered mouse models of schizophrenia[15,37,38,40,41]. These finding add further support for the genetic involvement of *ZIC2* in the pathogenesis of schizophrenia.

Regarding the basis of neural circuits underlying the higher brain function abnormalities observed in $Zic2^{kd/+}$mice, we consider the following two observations to be significant. Firstly, we observed a reduction in the number of cholinergic neurons in the basal forebrain, which raises the possibility that abnormal cholinergic regulation of higher brain function underlies the behavioral abnormalities seen in $Zic2^{kd/+}$ mice. Basal forebrain cholinergic neurons are thought to be capable of regulating the cortical processing of sensory stimuli within various domains[42]. In addition, recent studies indicate that the cholinergic system modulates cognitive deficits in schizophrenia and that cholinergic transmission is a potential target of therapeutics for the improvement of cognitive functions[43]. Thus, further evaluation of the cholinergic transmission dynamics in *Zic2* mutants would be beneficial for a better understanding of the role of Zic2 in cognitive function. We also examined the distribution of PV-positive cells in medial and dorsolateral prefrontal cortices and in the hippocampus (Figure S3) because the distribution of PV-positive cortical neurons, which represent a subset of GABAergic inhibitory neurons, is altered in some animal models of schizophrenia[40,44] and is thought to be a key abnormality underlying the pathogenesis of schizophrenia[45]. However, we did not observe any significant alterations in the distribution of PV-positive cells in $Zic2^{kd/+}$ cortices (Figure S3).

Our second key observation relates to those implying that abnormalities of the amygdala underlie the social behavior abnormalities in $Zic2^{kd/+}$ mice. The reduced aggressivity of $Zic2^{kd/+}$ mice was indicative of abnormal social behavior and we hypothesized that abnormalities of the amygdala were involved for a number of reasons. Firstly, it is well known that the amygdala is essential for controlling aggressive behaviors[46]. Also, lesions in the rat medial amygdala cause a reduction in aggressive behavior[47]. Adding further support, a recent study showed that the AHA and medial amygdala project into the hypothalamic aggression area (mediobasal hypothalamus), which plays a central role in the control of aggressive behavior[48]. These facts led us to hypothesize that the reduced aggressivity in $Zic2^{kd/+}$ mice is related to the altered morphology of AHA. However, there have been limited studies focusing on the role of AHA in aggressive behavior. Therefore, further investigation of the amygdalar abnormalities in $Zic2^{kd/+}$ mice would contribute to our understanding of the neural circuits controlling aggressive behavior.

The molecular mechanism of developmental disturbances that lead to the cholinergic neuronal loss and amygdalar dysgenesis remains elusive. As one interpretation, these abnormalities may reflect a milder representation of the HPE-like abnormality[8] and cortical dysgenesis partly as a result of the abnormal *Zic2*-expressing meningeal progenitor cells[11] in $Zic2^{kd/kd}$ mice. In terms of forebrain cholinergic neuron development, we found that the p75-expressing cholinergic progenitor neurons in the prospective medial septum and diagonal band are missing in *Zic1*/*Zic3* compound mutant mice[49]. Since the structure and function of the vertebrate Zic family of proteins is highly conserved[3], Zic2 might function to expand the medial forebrain cholinergic neural progenitor cells by inhibiting their exit from the proliferating cell cycle in a manner analogous to that in the *Zic1*/*Zic3* compound mutant mice[49].

Resequencing analysis of *Zic2* in Japanese patients with schizophrenia revealed three novel nonsynonymous mutations in *ZIC2*. Functional analysis of these mutations in the $Zic2^{kd/+}$ mouse model of schizophrenia indicated that the R409P mutation results in severe loss-of-function. We showed that the transcriptional activation capacity of the Zic2-R409P protein was about 20% that of the wild-type protein; which corresponds to the decreased protein production from the $Zic2^{kd}$ allele shown previously[8]. This finding in turn validates $Zic2^{kd/+}$ mice as an animal model of the R409P mutation in schizophrenia. The patient with the R409P mutation was diagnosed with residual-type schizophrenia.

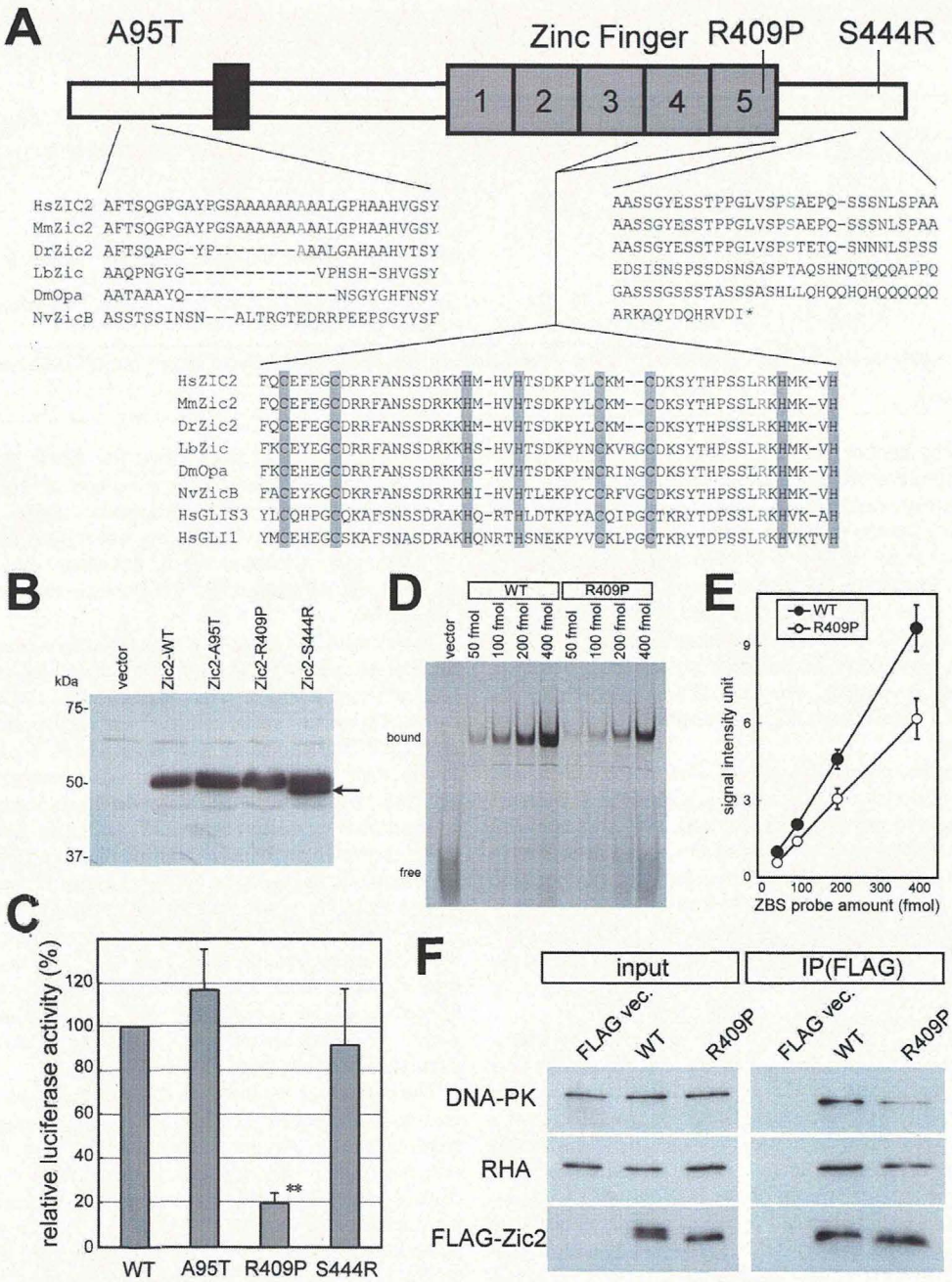


**Figure 6 | Properties of ZIC2 variants found in schizophrenia patients.** (A) Structure of the ZIC2 protein. Gray boxes with numbers indicate C2H2 motifs in the zinc finger domain of ZIC2. The positions of the A95T, R409P, and S444R mutations are indicated. Multiple alignments of the flanking regions of three mutations are indicated along with the reference sequences. Shaded characters show conserved cysteine and histidine residues in the C2H2 zinc fingers. Black box indicates an evolutionary conserved domain (ZOC, Zic-Opa-Conserved) domain. Gray characters indicate the mutated residues and the corresponding residues in other species (Hs, *Homo sapiens* [human]; Mm, *Mus musculus* [mouse]; Dr, *Danio rerio* [zebrafish]; Lb, *Loligo breekeri* [squid]; Dm, *Drosophila melanogaster* (fly); Nv, *Nematostella vectensis* [sea anemone]). (B) Immunoblotting of mouse wild-type Zic2 and Zic2 variants. NIH3T3 cells were transfected with the FLAG-tag expression plasmids. The Zic2 proteins were detected by the anti-FLAG antibody. Arrow indicates the fast migrating component in FLAG-Zic2-S444R. (C) NIH3T3 cells were transfected with a Zic2-responsive luciferase reporter vector together with a vector expressing wild-type FLAG-Zic2 (WT), or the FLAG-Zic2-A95T, -R409P, -S444R mutant proteins. All luciferase activities were normalized to the activities of the co-transfected elongation factor 1 promoter-driven Renilla luciferase. The means ± SEM of three independent experiments of three samples each are shown. (D) Gel mobility shift assay. IRD-labeled target DNAs were incubated with partially purified FLAG-Zic2-WT or FLAG-Zic2-R409P proteins expressed in 293T cells. The probes and the amount are indicated at the top. (E) Quantification of the gel shift assay result. Data are presented as means ± SEM. There were statistically significant differences between the FLAG-Zic2-WT and FLAG-Zic2-R409P-bound DNA probes at each dose (50 fmol, $P < 0.001$; 100 fmol, $P = 0.0022$; 200 fmol, $P = 0.012$; and 400 fmol, $P = 0.0089$). (F) FLAG-Zic2-WT or FLAG-Zic2-R409P expressed in 293T cells were immunoprecipitated with the anti-FLAG antibody. Proteins in the input cell lysates (input) and immunoprecipitates (IP) were analyzed by immunoblotting using anti-DNA-PK, anti-RHA, and anti-FLAG antibodies. There was a decrease in the amount of co-precipitated DNA-PK in FLAG-Zic2-R409P immunoprecipitates compared to those from FLAG-Zic2-WT, despite comparable amounts of FLAG-Zic2-R409P and FLAG-Zic2-WT.

Table 3 | Comparison of the morphological and behavioral features of *Zic2* kd/+ with those of other typical schizophrenia model mice.

| | Lateral ventricular volume | Anxiety | Novelty induced activity | Working memory | PPI | Social recognition | R-I aggression | Social interaction |
|---|---|---|---|---|---|---|---|---|
| Zic2 kd/+ | ↑ | = | ↑ | ↓ | ↓ | = | ↓ | = |
| DISC1-DN | ↑ | = | ↑ | = | ↓ | - | - | = |
| NRG1-TM | - | = | ↑ | = | ↓ | ↓ | ↑ | = |
| PV-ErbB4-/- | - | - | ↑ | ↓ | ↓ | - | - | - |

Dominant negative *Disc* transgenic (DISC1-DN) and *Nrg1* transmembrane knockout (NRG1-TM) results summary is based on [20]. Conditional knockout of *Erbb4* in PV-positive interneuron (PV-ErbB4-/-) is based on [39]. ↑, increased relative to WT; ↓, decreased relative to WT; =, no difference; -, not reported.

Many studies have investigated the *ZIC2* mutations in patients with HPE. A recent meta-analysis study of previously published results showed that the vast majority of *ZIC2* mutations (98%) cause significant loss-of-function[7]. This suggests that HPE is caused by severely impaired function of *ZIC2*. Interestingly, only the very few cases (three families), in which the function of *ZIC2* was shown to be null, included two independent parents with normal brain imaging despite the identification of *ZIC2* missense mutations (Q36P or D152F)[7]. Together with these results, our findings raise the possibility that mildly impaired ZIC2 function does not result in HPE, but in psychiatric illnesses.

In summary, behavioral and morphological phenotypes in $Zic2^{kd/+}$ mice were reminiscent of those of schizophrenia. Additionally, the detection of rare, but significantly defective, missense mutations in patients with schizophrenia suggests that further analysis of *ZIC2* in neuropsychiatric patients is meaningful. Since this study focused on missense mutations, there still remains the possibility that mutations in introns and/or flanking regions that provoke partial loss of function are associated with schizophrenia.

## Methods

**Animals.** Animal experiments were approved by the Animal Experiment Committee of the RIKEN Brain Science Institute (approval no. H22-EP068), and the mice were maintained by the institute's Research Resource Center. Mutant mice heterozygous for the $Zic2^{kd}$ allele ($Zic2^{kd/+}$) were described previously[8,9,12]. $Zic2^{kd}$ was generated by the insertion of the neomycin resistant cassette into an intron of mouse *Zic2*, resulting in the 20% of the wild-type allele[8], and were maintained in C57BL/6J background.

**Behavioral tests.** Home cage activity measurement, open field test, classical fear conditioning, Y-maze test were done as described[50,51].

**Resident-intruder test.** Group-reared mice were kept in isolation for 5 days before the test. The test was carried out in a dark phase (0:30 to 2:30) in a chamber that keeps the cage under dim (infrared) light at 25°C. Video recording from two opposite directions was initiated once the intruder mice had been gently placed in a vacant spot in the cage of the resident mice. The behaviors of the resident mouse were recorded for 10 min. The duration and number of times the resident mice spent sniffing, in active contact with, and in pursuit and attack with the intruder mice were measured by observers who were blinded to the genotypes of the mice.

**Social dominance tube test.** A wild type and a $Zic2^{kd/+}$ mice were placed in a head-to-head position first at the opposite ends of a clear plexiglass tube (3.4 cm inner diameter, 30 cm in length) in which two shutter plates were inserted at a distance of 13 cm from each end. The tests were begun by removing the shutters and ended when one mouse completely retreated from the tube. The mouse that retreated first was designated as the loser, and the remaining mouse was judged as the winner. The maximal test time was set to 2 min.

**Magnetic resonance imaging (MRI) based volumetric analysis.** MRI images of the adult male mice were acquired by subjecting anesthetized mice to an MRI scan using a vertical bore 9.4-T Bruker AVANCE 400WB imaging spectrometer (Bruker BioSpin, Rheinstetten, Germany). Animals were anesthetized with 3% and 1.5% isoflurane in air (2 L/min flow rate) for induction and maintenance, respectively. MRI images were obtained by using the FISP-3D protocol of Paravision software 5.0, by setting the following parameter values: Effective TE = 4.0 ms, TR = 8.0 ms, Flip angle = 15 degree, Average number = 5, Acquisition Matrix = 256 × 256 × 256, FOV = 25.6 × 25.6 × 25.6 mm. Manual measurements were made on the 3-dimensional (3D) MRI data to calculate total brain volume, hippocampus volume and lateral ventricle volume using the InsightITK-Snap software[52]. Regional volumetric changes were measured by voxel-based morphometry (VBM) using the Statistical Parametric Mapping (SPM) software package (http://www.fil.ion.ucl.ac.uk/spm/software/) for MATLAB (Mathworks, Natick, MA, USA) for pilot survey (data not shown).

**Histology and immunostaining.** Histological examination was done as described[9]. For the morphometric analysis, serial coronal sections were prepared, and analyzed at the following positions: +0.74 to +1.10 for the septum, diagonal band, striatum and the motor cortex; −0.34 to −0.82 for the substantia innominata, the basal nucleus of the Meynert, and the somatosensory cortex [anterior(+) to posterior(−) distance (mm) from bregma according to Paxinos et al.[53]]. The sections were stained with cresyl violet or by utilizing endogenous acetylcholine esterase activity[54] for histological examination.

Immunostaining was performed as previously described[55]. The primary antibodies were rabbit mouse anti-choline acetyltransferase (ChAT) polyclonal antibody (Chemicon, Temecula, CA, USA), mouse monoclonal anti-parvalbumin (PV) (Sigma, St. Louis, MO, USA), and rabbit anti-pan-Zic antibodies[10].

**Resequencing analysis of *ZIC2* in human subjects.** We performed resequencing analysis of *ZIC2* in 278 patients with schizophrenia who were of Japanese descent. The diagnosis of schizophrenia including the samples below was made on the basis of Diagnostic and Statistical Manual of Mental Disorders criteria (DSM-IV), by at least two expert psychiatrists. We then determined the allele frequencies of detected mutations using an expanded sample panel of schizophrenia patients (967 subjects: 457 men, 510 women; mean age 47.3 ± 13.8 [SD] years) and 1060 controls (502 men, 558 women; mean age 47.7 ± 13.6 years) who were documented as being free of mental disorders following brief interviews by expert psychiatrists. Our recruitment of schizophrenia and control subjects did not involve structured or semi-structured instruments. This study was approved by the ethics committees of RIKEN.

Protein-coding regions and exon/intron boundaries within the *ZIC2* gene were screened for polymorphisms by direct sequencing of PCR products using the BigDye Terminator v3.1 Cycle Sequencing kit (Applied Biosystems, Foster City, CA, USA) and the ABI PRISM 3730xl Genetic Analyzer (Applied Biosystems).

**Molecular and functional analysis.** Mouse *Zic2* variants that have the same missense mutations as the human *ZIC2* nonsynonymous mutations ($Zic2^{A95T}$ for $ZIC2^{A95T}$, $Zic2^{R408P}$ for $ZIC2^{R409P}$, and $Zic2^{S443R}$ for $ZIC2^{S444R}$) were generated by PCR[56] using pEFBOS-*Zic2*[31] or pcDNA3-HA-*Zic2* as templates. Hereinafter, we refer to them as *Zic2*-A95T ($Zic2^{A95T}$), *Zic2*-R409P ($Zic2^{R408P}$) and *Zic2*-S444R ($Zic2^{S443R}$), respectively. Expression plasmids for these wild-type *Zic2* and *Zic2* variants were constructed pcDNA3.1 (Invitrogen, Carlsband, CA, USA) and pCMVtag2 (Stratagene, La Jolla, CA, USA). pGL4-ZBS was constructed by inserting a mouse genomic DNA clone containing Zic2-binding sequences (Ishiguro et al., unpublished) into pGL4 (Promega, Madison, WI, USA). Cell culture, transfection, immunoblot analysis. luciferase reporter assay, gel shift assay, and immunoprecipitation were performed as previously described[31,33].

**Statistical analysis.** Parametric data were analyzed by using the two-sided Student's *t*-test (t-test) and non-parametric data were analyzed by using the Mann–Whitney's *U*-test (U-test). The *P* values refer to the t-test, unless otherwise specified. We also used the repeated measure two-way analysis of variance (RMANOVA) or the chi-square test for homogeneity. Differences were defined as statistically significant when $P < 0.05$.


1. Aruga, J. *et al.* The mouse zic gene family. Homologues of the Drosophila pair-rule gene odd-paired. *J Biol Chem* **271**, 1043–1047 (1996).
2. Nagai, T. *et al.* The expression of the mouse Zic1, Zic2, and Zic3 gene suggests an essential role for Zic genes in body pattern formation. *Dev Biol* **182**, 299–313 (1997).
3. Aruga, J. The role of Zic genes in neural development. *Mol Cell Neurosci* **26**, 205–221 (2004).
4. Grinberg, I. & Millen, K. J. The ZIC gene family in development and disease. *Clin Genet* **67**, 290–296, doi:10.1111/j.1399-0004.2005.00418.x (2005).
5. Merzdorf, C. S. Emerging roles for zic genes in early development. *Dev Dyn* **236**, 922–940 (2007).
6. Brown, S. A. *et al.* Holoprosencephaly due to mutations in ZIC2, a homologue of Drosophila odd-paired. *Nat Genet* **20**, 180–183 (1998).

7. Solomon, B. D. *et al.* Mutations in ZIC2 in human holoprosencephaly: description of a Novel ZIC2 specific phenotype and comprehensive analysis of 157 individuals. *J Med Genet* **47**, 513–524 (2010).
8. Nagai, T. *et al.* Zic2 regulates the kinetics of neurulation. *Proc Natl Acad Sci U S A* **97**, 1618–1623 (2000).
9. Aruga, J., Inoue, T., Hoshino, J. & Mikoshiba, K. Zic2 controls cerebellar development in cooperation with Zic1. *J Neurosci* **22**, 218–225 (2002).
10. Inoue, T., Ota, M., Mikoshiba, K. & Aruga, J. Zic2 and Zic3 synergistically control neurulation and segmentation of paraxial mesoderm in mouse embryo. *Dev Biol* **306**, 669–684 (2007).
11. Inoue, T., Ogawa, M., Mikoshiba, K. & Aruga, J. Zic deficiency in the cortical marginal zone and meninges results in cortical lamination defects resembling those in type II lissencephaly. *J Neurosci* **28**, 4712–4725 (2008).
12. Ogura, H., Aruga, J. & Mikoshiba, K. Behavioral abnormalities of Zic1 and Zic2 mutant mice: implications as models for human neurological disorders. *Behav Genet* **31**, 317–324 (2001).
13. Freedman, R. Schizophrenia. *N Engl J Med* **349**, 1738–1749 (2003).
14. Ross, C. A., Margolis, R. L., Reading, S. A., Pletnikov, M. & Coyle, J. T. Neurobiology of schizophrenia. *Neuron* **52**, 139–153 (2006).
15. Jaaro-Peled, H., Ayhan, Y., Pletnikov, M. V. & Sawa, A. Review of pathological hallmarks of schizophrenia: comparison of genetic models with patients and nongenetic models. *Schizophr Bull* **36**, 301–313 (2010).
16. Steen, R. G., Mull, C., McClure, R., Hamer, R. M. & Lieberman, J. A. Brain volume in first-episode schizophrenia: systematic review and meta-analysis of magnetic resonance imaging studies. *Br J Psychiatry* **188**, 510–518 (2006).
17. Vita, A., De Peri, L., Silenzi, C. & Dieci, M. Brain morphology in first-episode schizophrenia: a meta-analysis of quantitative magnetic resonance imaging studies. *Schizophr Res* **82**, 75–88 (2006).
18. Ellison-Wright, I., Glahn, D. C., Laird, A. R., Thelen, S. M. & Bullmore, E. The anatomy of first-episode and chronic schizophrenia: an anatomical likelihood estimation meta-analysis. *Am J Psychiatry* **165**, 1015–1023 (2008).
19. Karayiorgou, M., Simon, T. J. & Gogos, J. A. 22q11.2 microdeletions: linking DNA structural variation to brain dysfunction and schizophrenia. *Nat Rev Neurosci* **11**, 402–416 (2010).
20. Desbonnet, L., Waddington, J. L. & Tuathaigh, C. M. Mice mutant for genes associated with schizophrenia: common phenotype or distinct endophenotypes? *Behav Brain Res* **204**, 258–273 (2009).
21. Jaaro-Peled, H. *et al.* Neurodevelopmental mechanisms of schizophrenia: understanding disturbed postnatal brain maturation through neuregulin-1-ErbB4 and DISC1. *Trends Neurosci* **32**, 485–495 (2009).
22. Kellendonk, C., Simpson, E. H. & Kandel, E. R. Modeling cognitive endophenotypes of schizophrenia in mice. *Trends Neurosci* **32**, 347–358 (2009).
23. Pineda-Alvarez, D. E., Dubourg, C., David, V., Roessler, E. & Muenke, M. Current recommendations for the molecular evaluation of newly diagnosed holoprosencephaly patients. *Am J Med Genet C Semin Med Genet* **154C**, 93–101 (2010).
24. Brown, L. Y. *et al.* Holoprosencephaly due to mutations in ZIC2: alanine tract expansion mutations may be caused by parental somatic recombination. *Hum Mol Genet* **10**, 791–796 (2001).
25. Orioli, I. M. *et al.* Identification of novel mutations in SHH and ZIC2 in a South American (ECLAMC) population with holoprosencephaly. *Hum Genet* **109**, 1–6 (2001).
26. Dubourg, C. *et al.* Molecular screening of SHH, ZIC2, SIX3, and TGIF genes in patients with features of holoprosencephaly spectrum: Mutation review and genotype-phenotype correlations. *Hum Mutat* **24**, 43–51 (2004).
27. Roessler, E. *et al.* The full spectrum of holoprosencephaly-associated mutations within the ZIC2 gene in humans predicts loss-of-function as the predominant disease mechanism. *Hum Mutat* **30**, E541–554 (2009).
28. Aruga, J. *et al.* A wide-range phylogenetic analysis of Zic proteins: implications for correlations between protein structure conservation and body plan complexity. *Genomics* **87**, 783–792 (2006).
29. Pavletich, N. P. & Pabo, C. O. Crystal structure of a five-finger GLI-DNA complex: new perspectives on zinc fingers. *Science* **261**, 1701–1707 (1993).
30. Ramensky, V., Bork, P. & Sunyaev, S. Human non-synonymous SNPs: server and survey. *Nucleic Acids Res* **30**, 3894–3900 (2002).
31. Mizugishi, K., Aruga, J., Nakata, K. & Mikoshiba, K. Molecular properties of Zic proteins as transcriptional regulators and their relationship to GLI proteins. *J Biol Chem* **276**, 2180–2188 (2001).
32. Mizugishi, K. *et al.* Myogenic repressor I-mfa interferes with function of Zic family proteins. *Biochem Biophys Res Comm* **320**, 233–240 (2004).
33. Ishiguro, A., Ideta, M., Mikoshiba, K., Chen, D. J. & Aruga, J. ZIC2-dependent transcriptional regulation is mediated by DNA-dependent protein kinase, poly(ADP-ribose) polymerase, and RNA helicase A. *J Biol Chem* **282**, 9983–9995 (2007).
34. Arguello, P. A. & Gogos, J. A. Modeling madness in mice: one piece at a time. *Neuron* **52**, 179–196 (2006).
35. Stefansson, H. *et al.* Neuregulin 1 and susceptibility to schizophrenia. *Am J Hum Genet* **71**, 877–892 (2002).
36. O'Tuathaigh, C. M. *et al.* Phenotypic characterization of spatial cognition and social behavior in mice with 'knockout' of the schizophrenia risk gene neuregulin 1. *Neuroscience* **147**, 18–27 (2007).
37. Pletnikov, M. V. *et al.* Inducible expression of mutant human DISC1 in mice is associated with brain and behavioral abnormalities reminiscent of schizophrenia. *Mol Psychiatry* **13**, 173–186, 115 (2008).
38. Hikida, T. *et al.* Dominant-negative DISC1 transgenic mice display schizophrenia-associated phenotypes detected by measures translatable to humans. *Proc Natl Acad Sci U S A* **104**, 14501–14506 (2007).
39. Wen, L. *et al.* Neuregulin 1 regulates pyramidal neuron activity via ErbB4 in parvalbumin-positive interneurons. *Proc Natl Acad Sci U S A* **107**, 1211–1216, doi:10.1073/pnas.0910302107 (2010).
40. Shen, S. *et al.* Schizophrenia-related neural and behavioral phenotypes in transgenic mice expressing truncated Disc1. *J Neurosci* **28**, 10893–10904 (2008).
41. Chen, X. W. *et al.* DTNBP1, a schizophrenia susceptibility gene, affects kinetics of transmitter release. *J Cell Biol* **181**, 791–801 (2008).
42. Picciotto, M. R., Alreja, M. & Jentsch, J. D. in *Neuropsychopharmacology, the fifth generation of progress* (eds K. L. Davis, D. Charney, J. T. Coyle, & C. Nemerroff) 3–14. (Lippincott Williams & Wilkins, 2002).
43. Ross, R. G. *et al.* Research review: Cholinergic mechanisms, early brain development, and risk for schizophrenia. *J Child Psychol Psychiatry* **51**, 535–549 (2010).
44. Lodge, D. J., Behrens, M. M. & Grace, A. A. A loss of parvalbumin-containing interneurons is associated with diminished oscillatory activity in an animal model of schizophrenia. *J Neurosci* **29**, 2344–2354 (2009).
45. Gonzalez-Burgos, G., Hashimoto, T. & Lewis, D. A. Alterations of cortical GABA neurons and network oscillations in schizophrenia. *Curr Psychiatry Rep* **12**, 335–344.
46. Bear, M. F., Connors, B. W. & Paradiso, M. A. in *Neuroscience, exploring the brain* 572–583. (Lippincott Williams & Wilkins, 2007).
47. Vochteloo, J. D. & Koolhaas, J. M. Medial amygdala lesions in male rats reduce aggressive behavior: interference with experience. *Physiol Behav* **41**, 99–102 (1987).
48. Toth, M., Fuzesi, T., Halasz, J., Tulogdi, A. & Haller, J. Neural inputs of the hypothalamic "aggression area" in the rat.*Behav Brain Res* **215**, 7–20 (2010).
49. Inoue, T., Ota, M., Ogawa, M., Mikoshiba, K. & Aruga, J. Zic1 and Zic3 regulate medial forebrain development through expansion of neuronal progenitors. *J Neurosci* **27**, 5461–5473 (2007).
50. Katayama, K. *et al.* Slitrk1-deficient mice display elevated anxiety-like behavior and noradrenergic abnormalities. *Mol Psychiatry* **15**, 177–184, doi:10.1038/mp.2008.97 (2010).
51. Araya, R. *et al.* Loss of M5 muscarinic acetylcholine receptors leads to cerebrovascular and neuronal abnormalities and cognitive deficits in mice. *Neurobiol Dis* **24**, 334–344 (2006).
52. Yushkevich, P. A. *et al.* User-guided 3D active contour segmentation of anatomical structures: significantly improved efficiency and reliability. *Neuroimage* **31**, 1116–1128 (2006).
53. Paxinos, G. & Franklin, K. B. J. *The mouse brain in stereotaxic coordinates.* 2 edn, (Academic Press, 2001).
54. Vincent, S. R. in *Experimental neuroanatomy* (ed J. P. Bolam) Ch. 7, (Oxford University Press, 1992).
55. Aruga, J., Nozaki, Y., Hatayama, M., Odaka, Y. S. & Yokota, N. Expression of ZIC family genes in meningiomas and other brain tumors. *BMC Cancer* **10**, 79 (2010).
56. Fisher, C. L. & Pei, G. K. Modification of a PCR-based site-directed mutagenesis method. *Biotechniques* **23**, 570–571, 574 (1997).


## Acknowledgments

We thank the members of Aruga Laboratory for valuable discussions, Naoko Yamada, Yoshie Ito and Ryoko Takei for technical assistance, and Katsuhiko Mikoshiba for continuous encouragement of our Zic biology project. This work was supported by RIKEN BSI Funds and by a Grant-in-Aid for Scientific Research from the Ministry of Education, Culture, Sports, Science and Technology of Japan. A part of this study is the result of "Development of biomarker candidates for social behavior" carried out under the Strategic Research Program for Brain Sciences by the Ministry of Education, Culture, Sports, Science and Technology of Japan.

## Author contributions

M.H. and A.I. characterized the ZIC2 variants. Y.I., T.T. and T.Y. performed the resequencing analysis. A.I., N.T., K.S. Y.S.O., K.Y. and J.A. performed the behavioral analysis. K.S. performed the MRI analysis. Y. N. and J.A. performed the histological analysis. M.H., A.I., K.Y., T.Y. and J.A. wrote the manuscript.

## Additional information

**Supplementary Information** accompanies this paper at http://www.nature.com/scientificreports

**Competing financial interests:** The authors declare that there are no conflicts of interest associated with the present study.



**How to cite this article:** Hatayama, M. *et al. Zic2* hypomorphic mutant mice as a schizophrenia model and *ZIC2* mutations identified in schizophrenia patients *Sci. Rep.* 1, 16; DOI:10.1038/srep00016 (2011).

nature neuroscience

# Potent amyloidogenicity and pathogenicity of Aβ43

Takashi Saito[1,8], Takahiro Suemoto[1,8], Nathalie Brouwers[2,3], Kristel Sleegers[2,3], Satoru Funamoto[4], Naomi Mihira[1], Yukio Matsuba[1], Kazuyuki Yamada[5], Per Nilsson[1], Jiro Takano[1], Masaki Nishimura[6], Nobuhisa Iwata[1,7], Christine Van Broeckhoven[2,3], Yasuo Ihara[4] & Takaomi C Saido[1]

**The amyloid-β peptide Aβ42 is known to be a primary amyloidogenic and pathogenic agent in Alzheimer's disease. However, the role of Aβ43, which is found just as frequently in the brains of affected individuals, remains unresolved. We generated knock-in mice containing a pathogenic presenilin-1 R278I mutation that causes overproduction of Aβ43. Homozygosity was embryonic lethal, indicating that the mutation involves a loss of function. Crossing amyloid precursor protein transgenic mice with heterozygous mutant mice resulted in elevated Aβ43, impairment of short-term memory and acceleration of amyloid-β pathology, which accompanied pronounced accumulation of Aβ43 in plaque cores similar in biochemical composition to those observed in the brains of affected individuals. Consistently, Aβ43 showed a higher propensity to aggregate and was more neurotoxic than Aβ42. Other pathogenic presenilin mutations also caused overproduction of Aβ43 in a manner correlating with Aβ42 and with the age of disease onset. These findings indicate that Aβ43, an overlooked species, is potently amyloidogenic, neurotoxic and abundant *in vivo*.**



Alzheimer's disease, the most common form of dementia, is characterized by two pathological features in the brain, extracellular senile plaques and intracellular neurofibrillary tangles. Senile plaques consist of amyloid-β peptide (Aβ) that is generated from amyloid precursor protein (APP) through sequential proteolytic processing by β-secretase and γ-secretase. Two major forms of Aβ exist, Aβ40 and Aβ42, with Aβ42 being more neurotoxic as a result of its higher hydrophobicity, which leads to faster oligomerization and aggregation[1]. A number of mutations associated with early-onset familial Alzheimer's disease (FAD) have been identified in the *APP*, *PSEN1* and *PSEN2* genes, and these mutations lead to accelerated production of Aβ42 or an increase in the Aβ42/Aβ40 ratio. Together, these findings indicate that Aβ42 is essential for the initiation of pathogenesis. However, the possible involvement of longer Aβ species that also exist in the brains of individuals with Alzheimer's disease has not yet been fully investigated.

Thus far, various longer Aβ species, such as Aβ43, Aβ45, Aβ48, Aβ49 and Aβ50, have been qualitatively described in the brains of individuals with Alzheimer's disease[2]. Similar Aβ species have also been found in transgenic mice that overexpress *APP* carrying FAD-linked mutations[3]. Further quantitative studies have revealed that Aβ43 is deposited more frequently than Aβ40 in both sporadic Alzheimer's disease (SAD) and FAD[4–7].

How these Aβ species with different C-terminal ends are generated from the precursor has mainly been investigated by cell biological and biochemical methods. A number of studies[8,9] have found that γ and ε cleavage by γ-secretase controls the fate of the C-terminal end. Aβ43, generated from Aβ49 via Aβ46, is subsequently converted to Aβ40 by γ-secretase, whereas Aβ42 is independently generated from Aβ48 via Aβ45. It has also been reported that the FAD-associated I213T mutation in the *PSEN1* gene increases the generation of longer Aβ species, such as Aβ43, Aβ45 and those even longer than Aβ46, in addition to Aβ42 (ref. 10). It is also noteworthy that Aβ43 appears to be as prone to aggregate *in vitro* as Aβ42 (ref. 11), leading to faster formation of oligomers than occurs in the case of Aβ40 (ref. 12). These observations imply that Aβ43 could be produced as a physiological or pathological metabolite of γ-secretase and may affect Aβ amyloidosis in the brain.

To address whether Aβ43 contributes to Alzheimer's disease pathology, we decided to take advantage of the molecular phenotype of the presenilin-1 (PS1) R278I mutation, as this mutation results in selective overt production of Aβ43 *in vitro*[13], an effect that occurs to a much greater extent than in the case of other mutations, such as R278K, R278S and R278T. The R278I mutation has been independently reported in a pedigree bearing atypical Alzheimer's disease with language impairment[14]. A follow-up survey revealed that one of the affected individuals subsequently progressed to more severe cognitive impairment, and another individual from a different branch of the family with the mutation showed Alzheimer's disease–associated symptoms with an early loss of episodic memory and with a clinical onset of the disease at 59 years of age (M.N. Rossor, University College London, personal communication).

[1]Laboratory for Proteolytic Neuroscience, RIKEN Brain Science Institute, Wako-shi, Saitama, Japan. [2]Neurodegenerative Brain Diseases Group, Department of Molecular Genetics, Flanders Interuniversity Institute for Biotechnology, Antwerpen, Belgium. [3]Laboratory of Neurogenetics, Institute Born-Bunge, University of Antwerp, Antwerpen, Belgium. [4]Faculty of Life Sciences, Doshisha University, Kyoto, Japan. [5]Research Resource Center, RIKEN Brain Science Institute, Wako-shi, Saitama, Japan. [6]Molecular Neuroscience Research Center, Shiga University of Medical Science, Shiga, Japan. [7]Department of Molecular Medicinal Sciences, Division of Biotechnology, Nagasaki University Graduate School of Biomedical Sciences, Nagasaki, Japan. [8]These authors contributed equally to this work. Correspondence should be addressed T.C.S. (saido@brain.riken.jp).

Received 17 March; accepted 13 May; published online 3 July 2011; doi:10.1038/nn.2858

We generated PS1-R278I knock-in mice to assess the biological importance of the mutation and the pathological effect of Aβ43 on Aβ amyloidosis. Homozygosity in knock-in mice was embryonic lethal, presumably because of a partial loss of γ-secretase activity that resulted in a failure in Notch1 processing. Consistent with this, mouse embryonic fibroblasts (MEFs) derived from the homozygous knock-in mice exhibited a failure in PS1 endoproteolysis and Notch1 processing, implying that the particular selectivity of the PS1-R278I mutation for Aβ43 production is closely associated with the partial loss of γ-secretase activity, that is, suppression of the Aβ43-to-Aβ40 conversion, which could also be caused by some of the other PS1 mutations. We crossed heterozygous knock-in mice with APP transgenic mice (APP23 mice carrying the human *APP* isoform 751 transgene harboring the Swedish mutation (K651N M652L)) and found that the progeny exhibited short-term memory loss before plaque formation and developed considerably accelerated amyloid pathology, indicating that Aβ43 is potently amyloidogenic and pathogenic *in vivo*.

## RESULTS

### Generation of PS1-R278I knock-in mice

To generate PS1 knock-in mice, we constructed a targeting vector carrying a point mutation that results in the replacement of arginine 278 to isoleucine in exon 8 of the *PSEN1* allele (**Supplementary Fig. 1a**). Homologous recombination, germline transmission and genotype were confirmed by Southern blotting and PCR (**Supplementary Fig. 1b,c**). The expression levels of the mutant and wild-type PS1 in the embryonic mouse brains were identical (**Supplementary Fig. 1d**). Unexpectedly, homozygous knock-in (R278I/R278I) was embryonic lethal at embryonic day 15–18 (E15–18; **Fig. 1a**). The mutant embryos showed an overall size reduction, a stubby tail, limb ateliosis and hemorrhage in the CNS as compared with wild-type littermate controls (**Fig. 1a**).

This phenotype is similar to that of PS1-deficient mice and Notch1-related mutant mice[15,16], although the adverse phenotype of the PS1-R278I knock-in mice appeared a few days later than that of PS1-deficient mice. In contrast, we observed no developmental deficits in heterozygous knock-in (+/R278I) mice (**Fig. 1a** and **Supplementary Fig. 2**). The lethal phenotype of the R278I mutation appears to be caused by a loss of developmental function that manifests only under the recessive condition. We generated two lines of double-mutant mice: R278I knock-in/PS1 knockout and M146V knock-in/PS1 knockout. The phenotype of former was embryonic lethal and the latter was normal (**Supplementary Fig. 3a–d**). This observation suggests that the R278 mutation is a loss-of-function mutation. To the best of our knowledge, this is the first case of developmental abnormality being caused by a FAD-linked PS1 point mutation.



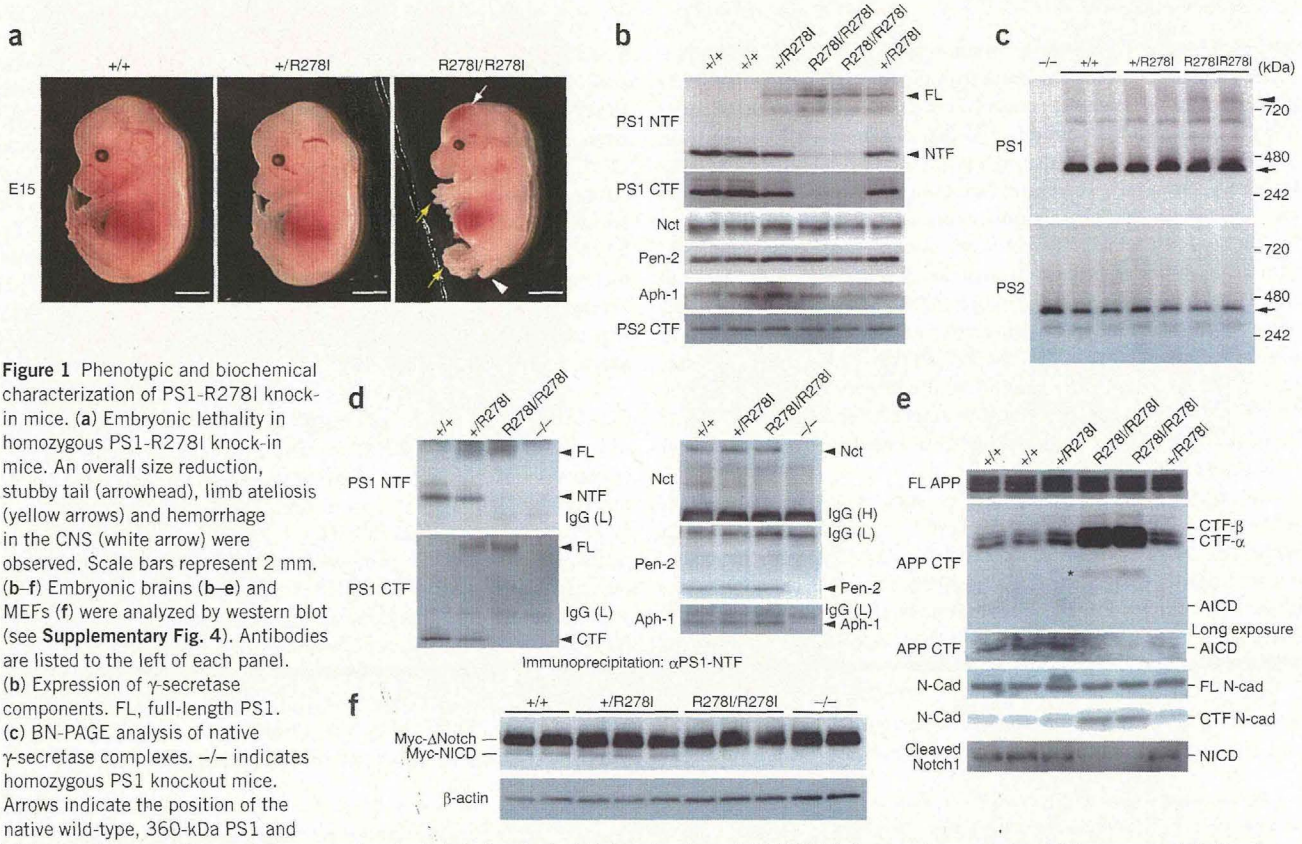


**Figure 1** Phenotypic and biochemical characterization of PS1-R278I knock-in mice. (**a**) Embryonic lethality in homozygous PS1-R278I knock-in mice. An overall size reduction, stubby tail (arrowhead), limb ateliosis (yellow arrows) and hemorrhage in the CNS (white arrow) were observed. Scale bars represent 2 mm. (**b–f**) Embryonic brains (**b–e**) and MEFs (**f**) were analyzed by western blot (see **Supplementary Fig. 4**). Antibodies are listed to the left of each panel. (**b**) Expression of γ-secretase components. FL, full-length PS1. (**c**) BN-PAGE analysis of native γ-secretase complexes. –/– indicates homozygous PS1 knockout mice. Arrows indicate the position of the native wild-type, 360-kDa PS1 and PS2 γ-secretase complexes, whereas arrowhead points to the atypical high molecular weight (750 kDa) γ-secretase complex. (**d**) Immunoprecipitation by antibodies to PS1-NTF. IgG(H) and IgG(L) indicate immunoglobulin heavy and light chains, respectively. (**e**) γ-secretase activity in PS1-R278I knock-in brains. Brain extracts were analyzed by western blotting to detect endogenous APP CTF-β, APP CTF-α, APP intracellular domain (AICD), full-length N-cadherin, N-cadherin CTF and NICD products. * indicates an additional signal, smaller than that of CTF-α, which appeared in the knock-in mice. (**f**) Notch1 processing in PS1-R278I knock-in MEFs. Myc-tagged ΔNotch was transiently expressed in the MEFs, and cell lysates were subjected to western blot analysis using antibody to Myc. β-actin levels are shown as internal controls.

### Abnormal PS1 endoproteolysis and Notch1 processing

To assess the functional importance of the R278I mutation in the PS1 knock-in line, we analyzed the biochemical properties of PS1-R278I γ-secretase in the embryonic brains before degeneration (**Fig. 1a**). Western blotting revealed a marked decrease in the levels of the N-terminal fragment (NTF) and C-terminal fragment (CTF) of PS1, indicating a failure of PS1 endoproteolysis, in homozygous knock-in brains, whereas the γ-secretase components, including Nicastrin (Nct), presenilin enhancer-2 (Pen-2) and anterior pharynx defective-1 protein (Aph-1), were expressed at normal levels (**Fig. 1b**). The NTF and CTF in the homozygous knock-in mice were, however, clearly detectable, indicating that a fraction of the endoproteolytic activity of PS1 still remained (**Fig. 1b** and **Supplementary Fig. 3e**). It is also noteworthy that the endoproteolysis was partially blocked in the heterozygous PS1-R278I brain, suggesting that the process is at least partly autolytic.

We next investigated whether the PS1-R278I mutation affects the assembly of the γ-secretase complex by Blue Native PAGE (BN-PAGE)[17]. A major signal corresponding to a molecular weight of 360 kDa, the normal molecular weight of the native PS1 γ-secretase complex, was detected in both wild-type and knock-in brains in a manner similar to that of the PS2 γ-secretase complex (**Fig. 1c**). Immunoprecipitation experiments further demonstrated that the mutant PS1 formed a complex with Nct, Pen-2 and Aph-1 (**Fig. 1d**). These data indicate that the PS1-R278I mutation does not affect the formation of the γ-secretase complex. Notably, BN-PAGE detected a minor signal corresponding to a higher molecular weight of 750 kDa in the homozygous knock-in brains (**Fig. 1c**). A similar higher molecular weight signal has been described in preparations from an individual with a deletion of exon 9 in the *PSEN1* gene (PS1-ΔE9)[17] and from SH-SY5Y cells treated with a γ-secretase inhibitor, L-685,458 (ref. 18). PS1-ΔE9 and PS1-ΔT440 also cause PS1 endoproteolytic abnormality in a similar manner to the PS1-R278I mutation[19–21]. The presence of this high molecular weight γ-secretase may reflect a conformational change in the multicomponent complex or binding of additional factor(s) to the complex, although its mechanistic involvement remains unclear.

We then examined the effect of the mutation on the metabolism of the γ-secretase substrates. Both the CTF-α and CTF-β of APP and the CTF of N-cadherin accumulated at substantial levels in the homozygous PS1-R278I knock-in mouse brain, but not in the wild-type or heterozygous brains (**Fig. 1e**). Conversely, the APP intracellular domain and Notch1 intracellular domain (NICD) could not be detected in the homozygous knock-in. An additional signal smaller than that of CTF-α appeared in the knock-in mice (**Fig. 1e**), presumably representing an aberrant proteolytic product of CTF-α and CTF-β. These data indicate that the PS1-R278I mutation leads to a substantial loss of γ-secretase activity in a recessive manner.

To further analyze the mutant γ-secretase, we established MEFs from knock-in mice and littermate controls. Western blotting (**Supplementary Fig. 4a**), BN-PAGE (**Supplementary Fig. 4b**) and immunoprecipitation experiments (**Supplementary Fig. 4c**) revealed that the biochemical properties of mutant presenilin in MEFs were

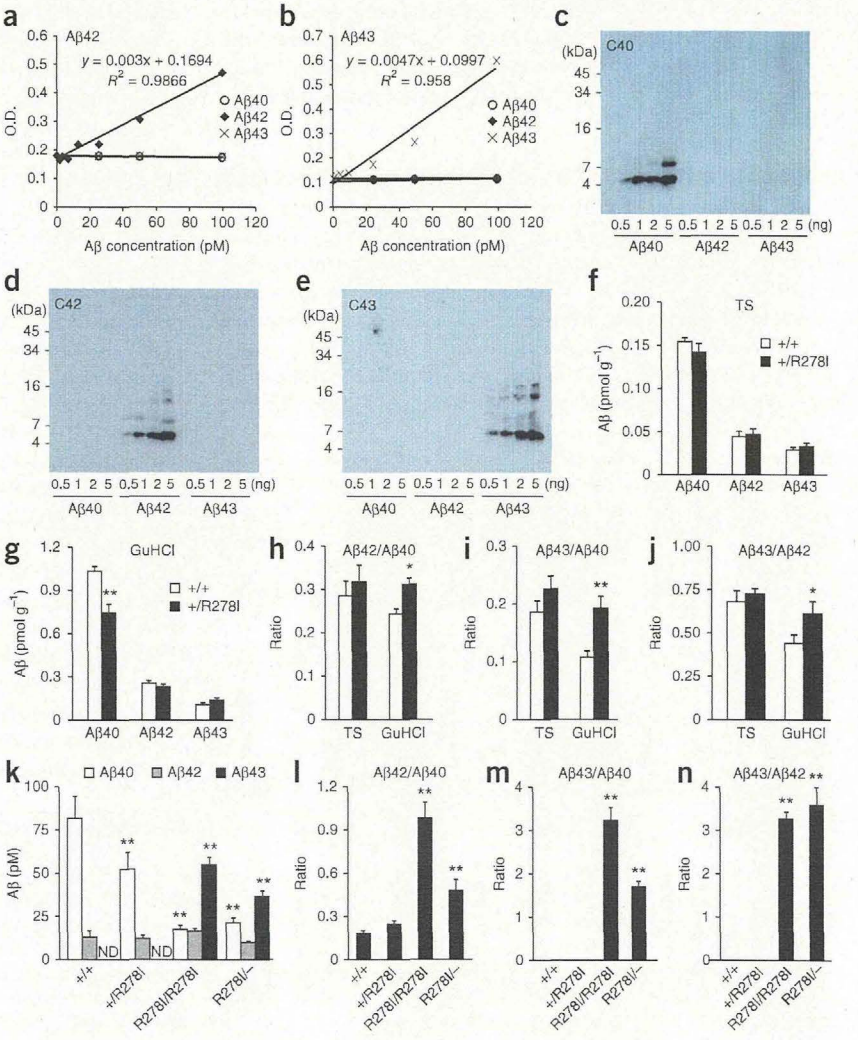


**Figure 2** Aβ levels in adult PS1-R278I knock-in mouse brains and MEFs. (**a**,**b**) Establishment of ELISA system to specifically quantify Aβ42 and Aβ43 (see **Supplementary Figs. 6a**,**b** and **7**). (**c–e**) Specificity of the antibodies to Aβ40, Aβ42 and Aβ43 used in this ELISA system. Synthetic Aβ1–40, Aβ1–42 and Aβ1–43 were separated by tris/tricine PAGE (15% polyacrylamide gel) and subjected to western blotting. Antibodies to Aβ C40, C42 and C43 specifically recognized Aβ1–40, Aβ1–42 and Aβ1–43, respectively (see **Supplementary Fig. 6c–e**). (**f–n**) Quantification of Aβ40, Aβ42 and Aβ43 by ELISA in adult mouse brains (**f–j**) and MEFs (**k–n**). (**f–j**) Cortical hemispheres from 24-month-old wild-type and heterozygous knock-in mice were homogenized and fractionated into Tris-HCl–buffered saline–soluble (TS) and GuHCl-soluble fractions. Data represent mean ± s.e.m. ($n = 9$). $^{*}P < 0.05$ and $^{**}P < 0.01$ between wild-type and heterozygous knock-in mice, Student's $t$ test. (**k–n**) Aβ concentrations in conditioned medium from MEFs. We inoculated $8 \times 10^5$ cells in a 1-ml culture. The conditioned medium was collected after 24 h and subjected to ELISA. R278I/– indicates a double heterozygote PS1-R278I knock-in × PS1 knockout mice. Data represent mean ± s.d. from two independent experiments ($n = 16$). $^{**}P < 0.01$ compared with wild type, one-way ANOVA with Scheffe's $F$ test. ND, not detected.

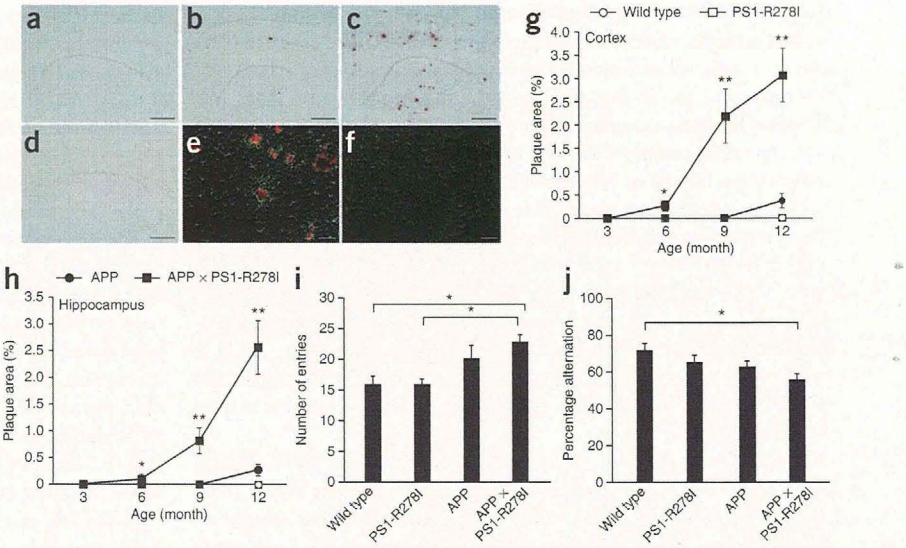


**Figure 3** Acceleration of Aβ pathology and short-term memory impairment by the R278I knock-in mutation in APP mice. (**a**–**f**) Brain sections from APP × PS1-R278I mice (3 (**a**), 6 (**b**) and 9 months (**c**,**d**) old) and 9-month-old single APP mice (**d**,**f**) were immunostained with the 4G8 antibody to Aβ (**a**–**d**) and antibody to GFAP (green) with 4G8 counterstaining (red) (**e**,**f**). Aβ-immunostained brain sections from cortex (**g**) and hippocampus (**h**) of 3-, 6-, 9- and 12-month-old wild-type, APP and heterozygous PS1-R278I knock-in mice, as well as APP × PS1-R278I mice were analyzed ($n = 5$–6 each genotype). $^*P < 0.05$ and $^{**}P < 0.01$ compared with APP mice, two-way ANOVA with Scheffe's $F$ test. Scale bars represent 500 μm (**a**–**d**) and 50 μm (**e**,**f**). (**i**,**j**) Y-maze test was performed before plaque formation using 3–4-month-old male wild-type, PS1-R278I knock-in, APP and APP × PS1-R278I mice. Data represent mean ± s.e.m. ($n = 10$ each genotype). $^*P < 0.05$ compared with wild-type or PS1-R278I knock-in mice, one-way ANOVA with Scheffe's $F$ test.

identical to those in the embryonic brains. We then expressed Myc-tagged ΔNotch1 in the mutant and wild-type MEFs. Western blot analysis revealed that conversion of Myc-ΔNotch1 to Myc-NICD by limited proteolysis occurred in wild-type and heterozygous knock-in MEFs, but not in the homozygous knock-in or PS1 knockout MEFs (**Fig. 1f**). These results indicate that the R287I mutation induces developmental deficits by abolishing of γ-secretase–dependent Notch1 processing.

### Aβ40, Aβ42 and Aβ43 in PS1-R278I knock-in brains and MEFs

Because homozygous R278I knock-in mice are embryonic lethal, we went on to analyze adult heterozygous knock-in mice. The adult heterozygous mice were normal in terms of development and anatomy at both 3 and 24 months of age (**Supplementary Fig. 2**), whereas various biochemical properties of PS1, such as partial abnormality of endoproteolysis, the molecular weight of γ-secretase and the identity of the complex components, were identical to those of the heterozygous embryonic brain (**Supplementary Fig. 5**). We then established a specific and highly sensitive ELISA system that could distinguish between Aβ40, Aβ42 and Aβ43 over a broad concentration range (**Fig. 2a**,**b** and **Supplementary Figs. 6a**,**b** and **7**). The antibodies that we used were highly specific to each Aβ species (**Fig. 2c**–**e** and **Supplementary Fig. 6c**–**e**). Brain tissue fractions that were soluble in Tris-HCl–buffered saline and those that were soluble in 6 M guanidine-HCl (GuHCl) were subjected to quantification.

There was a significant decrease in the steady-state levels of Aβ40 in the GuHCl-soluble fraction in the brains of aged (24 months old) heterozygous PS1-R278I knock-in mice as compared with wild-type animals ($P < 0.01$), although no differences were recorded in the levels of Aβs in the Tris-HCl–buffered saline fraction, or in the levels of Aβ42 and Aβ43 in the GuHCl-soluble fraction (**Fig. 2f**,**g**). This reduction of Aβ40 in the GuHCl-soluble fraction resulted in a significant elevation of the Aβ42/Aβ40 ($P < 0.05$) and Aβ43/Aβ40 ($P < 0.01$) ratios in the GuHCl-soluble fraction (**Fig. 2h**,**i**). Notably, the Aβ43/Aβ42 ratio was also significantly increased in the GuHCl-soluble fraction of the heterozygous PS1-R278I knock-in mouse brain ($P < 0.05$; **Fig. 2j**). In younger PS1-R278I knock-in mice (3 months old), Aβ43 levels were too low to detect, although the GuHCl-Aβ40 levels were again significantly reduced in the knock-in mice ($P < 0.05$; **Supplementary Fig. 8**). These results indicate that Aβ43 levels in the mouse brain increase on aging, and that the increase in the Aβ42/Aβ40 and Aβ43/Aβ40 ratios observed in the older heterozygous mice appears to be primarily caused by a decrease in Aβ40. Furthermore, the R278I mutation led to an elevation in the Aβ43/Aβ42 ratio in aged mice. Taken together, these findings indicate that the PS1-R278I mutation gives rise to a modest *in vivo* effect in terms of the levels of endogenous Aβ species under heterozygous conditions.

We next quantified the Aβ variants in conditioned medium from knock-in MEFs (**Fig. 2k**–**n**). The steady-state levels of Aβ40 were

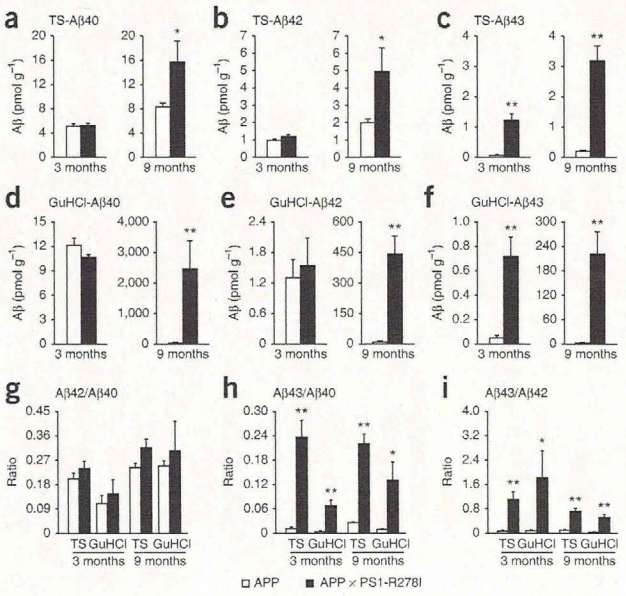


**Figure 4** Aβ40, Aβ42 and Aβ43 in APP × PS1-R278I mice. (**a**–**i**) The levels of Aβ40 (**a**,**d**), Aβ42 (**b**,**e**) and Aβ43 (**c**,**f**) were quantified by ELISA and the ratios of the Aβ species (**g**–**i**) were subsequently determined. Cortical hemispheres from single APP and APP × PS1-R278I mouse brain (3 and 9 months old) were homogenized and fractionated into Tris-HCl–buffered saline–soluble fractions (**a**–**c**) and GuHCl-extractable fractions (**d**–**f**). Data represent mean ± s.e.m. ($n = 7$, 3 months old; $n = 5$, 9 months old). $^*P < 0.05$ and $^{**}P < 0.01$ between APP mice and APP × PS1-R278I mice, Student's $t$ test.

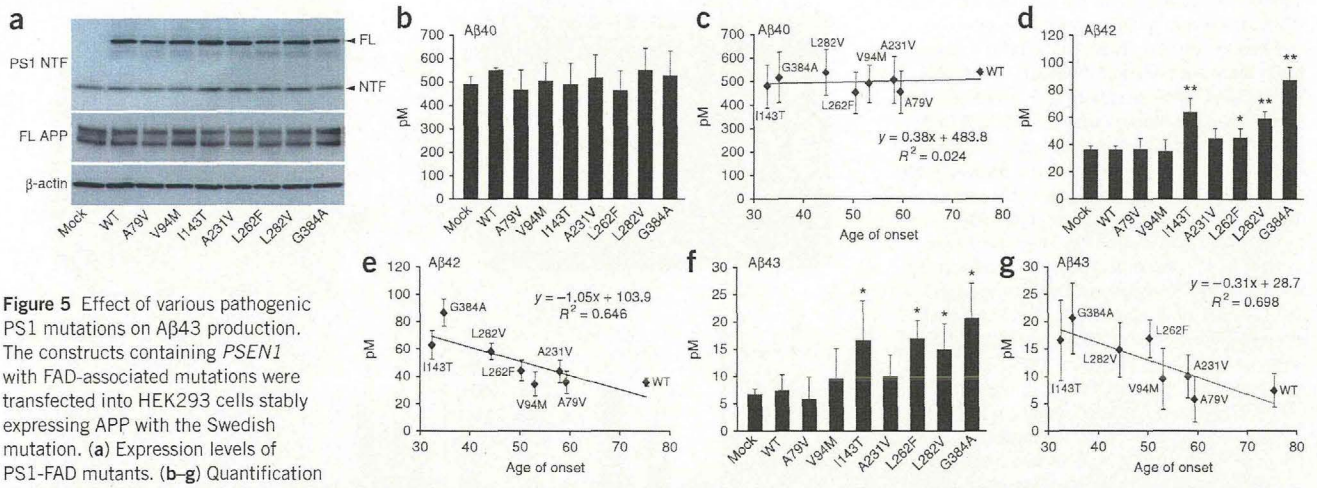


**Figure 5** Effect of various pathogenic PS1 mutations on Aβ43 production. The constructs containing *PSEN1* with FAD-associated mutations were transfected into HEK293 cells stably expressing APP with the Swedish mutation. (**a**) Expression levels of PS1-FAD mutants. (**b–g**) Quantification of the steady-state levels of Aβ40, Aβ42 and Aβ43 and the correlation between Aβ levels and the age of disease onset. Age of onset is shown as follows: wild type (WT, 75 years old), A79V (59.3), V94M (53), I143T (32.5), A231V (58), L262F (50.3), L282V (44) and G384A (34.9)[24,44]. Data represent mean ± s.d. from five independent series each consisting of duplicate measurements. $*P < 0.05$ and $**P < 0.01$ compared with wild type, one-way ANOVA with Dunnett test.

significantly reduced in a gene dose–dependent manner in the PS1-R278I MEFs as compared with wild-type MEFs ($P < 0.01$). In contrast, Aβ43 markedly increased in the homozygous knock-in MEFs, whereas Aβ42 levels remained unchanged in all genotypes (**Fig. 2k**). Thus, the ratios of longer Aβ species significantly increased in homozygous PS1-R278I knock-in MEFs ($P < 0.01$; **Fig. 2l–n**). Notably, there was no increase in Aβ43 levels in conditioned medium from heterozygous knock-in MEFs (**Fig. 2k**). To unravel the underlying mechanism, we crossed heterozygous R278I knock-in mice with PS1 knockout mice (R278I/–) and measured the levels of Aβs present in conditioned medium from cultured MEFs. Aβ43 levels were increased, implying that wild-type PS1 processes Aβ43 to Aβ40 in heterozygous PS1-R278I knock-in MEFs (**Fig. 2k**). Furthermore, no Aβ43 was detected in heterozygous PS1 knock-out MEFs (data not shown). Together, the data suggests that the γ-secretase substrate can be transferred between separate PS1 molecules or between dimers of PS1, as previously suggested[22], or even between PS1 molecules in the PS1 complexes, for further processing. The fact that total Aβ (Aβ40 + Aβ42 + Aβ43) was decreased in heterozygous knock-in MEFs, as compared with homozygous knock-in MEFs, is of particular interest. This might be a result of a dysfunctional PS1 heterodimer, with wild-type PS1 being either directly affected by PS1-R278I or overloaded with Aβ43 generated by PS1-R278I. Further experiments are required to resolve the reason behind the decreased total Aβ level (**Fig. 2k** and **Supplementary Fig. 9b**). Taken together, our data indicate that the R278I mutation

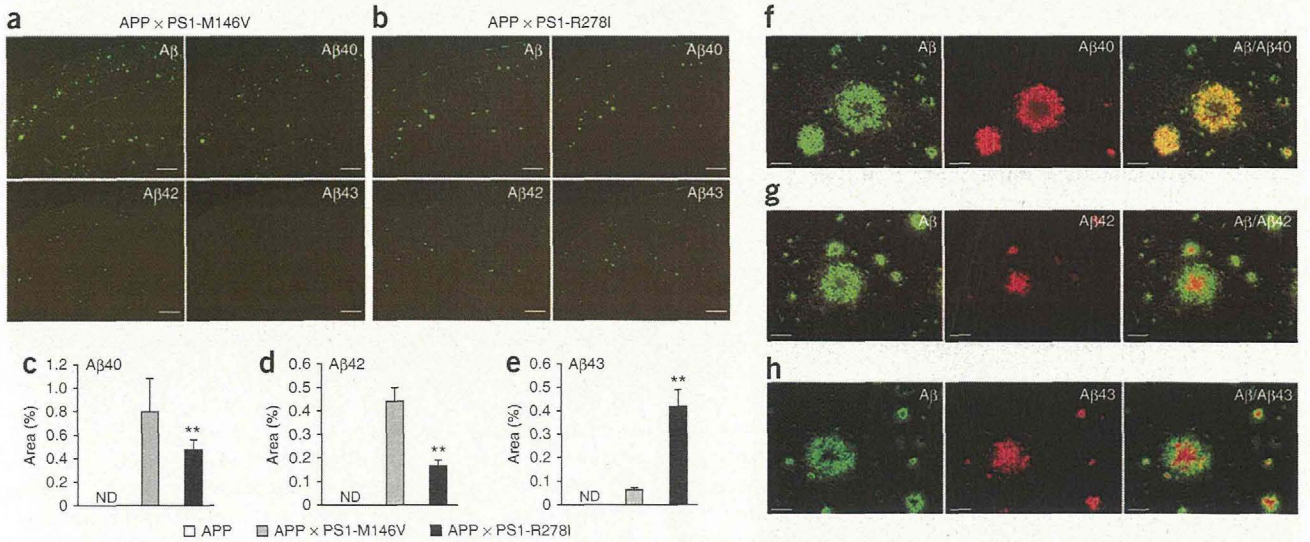


**Figure 6** Localization of Aβ species in amyloid plaques of APP × PS1-R278I mice. (**a,b**) A set of serial brain sections from 9-month-old APP × PS1-M146V mice (**a**) and APP × PS1-R278I mice (**b**) were immunostained with the following antibodies to Aβ: 4G8 (total Aβ), C40 (Aβ1–40), C42 (Aβ1–42) and C43 (Aβ1–43). (**c–e**) The immunoreactive areas in single APP (left), APP × PS1-M146V (middle) and APP × PS1-R278I (right) mice were quantified as indicated ($n = 6$). $**P < 0.01$ between APP × PS1-M146V mice and APP × PS1-R278I mice, one-way ANOVA with Scheffe's $F$ test. ND, not detected. (**f–h**) Double-staining with 4G8 (green) and Aβ40 (**f**), Aβ42 (**g**) or Aβ43 (**h**) (red). The images in the left (green) and middle (red) are merged (yellow) on the right. Scale bars represent 500 μm (**a,b**) and 50 μm (**f–h**).

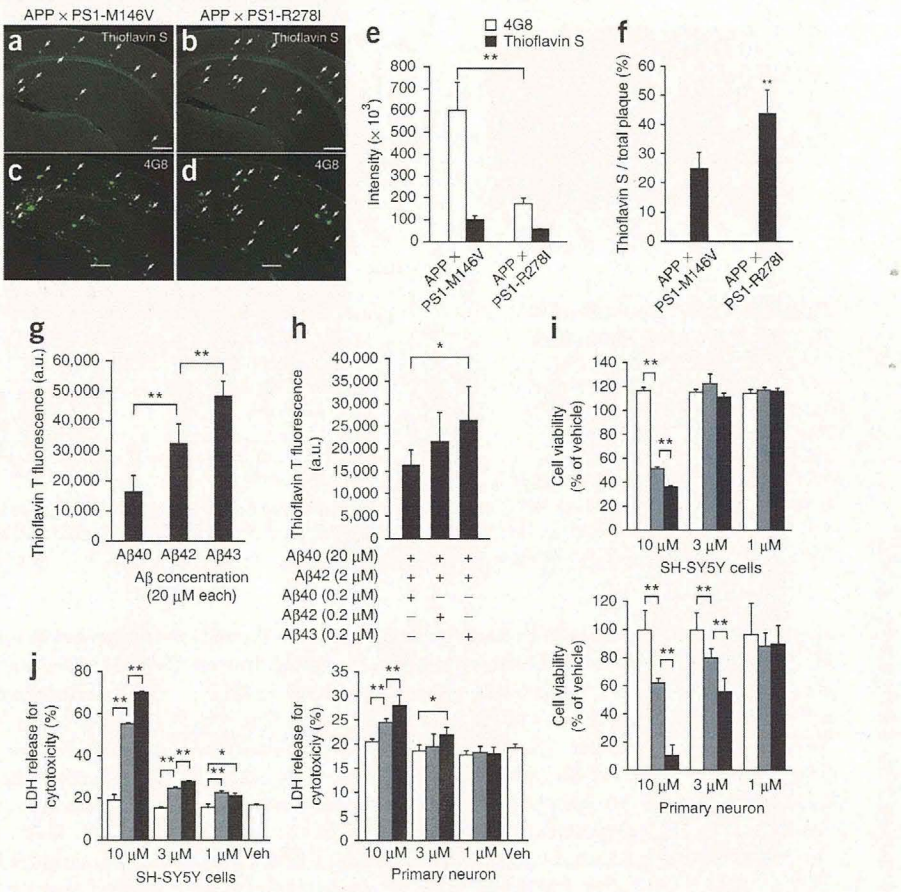


**Figure 7** Mature amyloid plaques in APP × PS1-R278I mice and *in vitro* aggregation property and neural cell toxicity of Aβ43. (**a**–**f**) A set of serial brain sections from 9-month-old APP × PS1-M146V mice (**a**,**c**) and APP × PS1-R278I mice (**b**,**d**) were stained with thioflavin S (**a**,**b**) and immunostained with 4G8 (**c**,**d**). Thioflavin S–positive plaque are marked with arrows (**a**,**b**) and the corresponding plaques in the serial brain sections are also marked (**c**,**d**). Scale bars represent 500 μm. (**e**,**f**) The intensity of cortical and hippocampal Aβ immunoreactivity and thioflavin S signals were quantified (**e**), and the ratio of thioflavin S/total Aβ signal of amyloid plaques was determined (**f**) ($n = 12$). Data represent mean ± s.e.m. $^{**}P < 0.01$ between APP × PS1-M146V mice and APP × PS1-R278I mice, Student's *t* test. (**g**,**h**) *In vitro* Aβ aggregation experiments. Incorporation of thioflavin T into Aβ aggregates was measured by fluorescence spectroscopy. The aggregation properties of 20 μM Aβ40, Aβ42 and Aβ43 at 20 μM were measured individually in **g**. The effect of Aβ40, Aβ42 and Aβ43 at a concentration of 0.2 μM on the mixture of 20 μM Aβ40 and 2 μM Aβ42 was then assessed in **h**. Data represent mean ± s.d. from three independent series each consisting of 6–8 individual measurements. $^{**}P < 0.01$ between Aβ40 and Aβ42 or between Aβ42 and Aβ43, $^{*}P < 0.05$ between Aβ40 and Aβ43, one-way ANOVA with Scheffe's *F* test. (**i**,**j**) Neural cell toxicity of Aβ43. Cell viability (**i**) and lactate dehydrogenase (LDH) release as a measure of cell toxicity (**j**) were assayed. Aβs were administrated at 1, 3 and 10 μM, respectively. The results obtained after treatment with Aβ40 (white), Aβ42 (gray) and Aβ43 (black) are indicated, and vehicle (veh) treatment was also indicated by open column in (**j**). Data represent mean ± s.d. from three independent series each consisting of six individual measurements. $^{**}P < 0.01$ between Aβ40 and Aβ42 or between Aβ42 and Aβ43, and $^{*}P < 0.05$ between Aβ40 and Aβ43, two-way ANOVA with Scheffe's *F* test or Dunnett test.



inhibits Aβ43 to Aβ40 conversion, leading to increased Aβ43 levels and concomitant decrease of Aβ40 without altering Aβ42 levels. A similar Aβ-processing pathway has been described previously[9] (**Fig. 2k** and **Supplementary Fig. 10**).

### Aβ pathology and memory impairment of APP mice

Overexpression of wild-type human APP in the above-stated MEFs using a semliki-forest virus vector[23] resulted in a significant increase in Aβ43 in the heterozygous R278I knock-in cells ($P < 0.05$; **Supplementary Fig. 9**). The presence of the excessive γ-secretase substrates, that is, APP CTF-α and CTF-β, appeared to force the mutant PS1 to participate in APP processing. These observations prompted us to crossbreed heterozygous PS1-R278I knock-in mice with APP mice to assess the effect of Aβ43 *in vivo*. APP × PS1-R278I mice started to accumulate pathological Aβ deposits at around 6 months of age, whereas it took about 12 months for APP transgenic mice to begin to show signs of such deposition (**Fig. 3a**–**h**). Massive astrocytosis was also detected around the amyloid plaques by 9 months age in the APP × PS1-R278I mice, but not in single transgenic mice (**Fig. 3e**,**f**). Behaviorally, 3–4-month-old APP × PS1-R278I mice exhibited short-term memory impairment as compared with single transgenic mice when their performance was evaluated in a Y-maze test (**Fig. 3i**,**j**). A similar tendency was also observed in the Morris water-maze test, although the difference in this case did not reach statistical significance ($P = 0.051$; data not shown). Taken together, these findings indicate that the PS1-R278I mutation leads to accelerated Aβ pathology with an accompanying inflammatory response and that the cognitive impairment occurs even before plaque formation.

We next quantified the steady-state levels of Aβ40, Aβ42 and Aβ43 in the brains of APP and APP × PS1-R278I mice at 3 and 9 months. Notably, only the double-mutant mice exhibited selective elevation of Aβ43 in both Tris-HCl–buffered saline–soluble and GuHCl-soluble brain fractions at 3 months, which is a time before the pathological deposition of Aβ (**Fig. 4a**–**f**), but by which the double-mutant mice already showed short-term memory impairment (**Fig. 3i**,**j**). In contrast, Aβ40 and Aβ42 levels started to increase at around 9 months. Consequently, both the Aβ43/Aβ40 and Aβ43/Aβ42 ratios were higher in the double mutant mice than in the single APP transgenic mice at both 3 and 9 months, whereas the Aβ42/Aβ40 ratio remained unaltered (**Fig. 4g**–**i**). It is worth noting that the elevation of biochemically detectable Aβ43 levels preceded plaque formation, implying that Aβ43 may be the initial seeding species and the trigger of memory impairment in this mouse model. The steady-state level of Aβ43 also increased in an age-dependent manner in the single APP transgenic mouse brains, beginning before plaque formation (**Fig. 3g**,**h** and **Supplementary Fig. 11**).

In addition, we observed that a variety of FAD-associated PS1 mutations resulted in overproduction of Aβ43 in a manner correlating with